

Effect of Inclination Grooves on Axial Flow Compressor Stability: An Experimental and Numerical Simulation Study

W. H. Liu, W. L. Chu[†], H. G. Zhang and C. Y. Zhang

School of Power and Energy, Northwestern Polytechnical University, Xi'an, Shanxi, 710129, China

[†]Corresponding Author Email: wlcchu@nwpu.edu.cn

(Received June 12, 2022; accepted September 27, 2022)

ABSTRACT

In the present study, various groove casing treatments were evaluated under a high-speed subsonic axial flow compressor using experimental and numerical simulation methods. The aim of this study was to explore the effect of inclination of grooves on compressor stability and performance. The potential flow mechanisms were also evaluated. Three different inclination grooves were designed in this study: grooves with no inclination, grooves with 30 degrees upstream inclination and grooves with 30 degrees downstream inclination. Similar effect of the grooves on the compressor stability and efficiency was observed under experimental and numerical analyses. The grooves with no inclination, 30 degrees upstream inclination and 30 degrees downstream inclination enhanced stall margin by 6.08%, 8.74% and 3.03%, respectively. The peak efficiency losses of the three types of grooves were 1.62%, 0.94% and 2.33%, respectively. Tip flow field analyses demonstrated that the radial transport effect caused by grooves effectively reduced tip loads and alleviated tip blockage. This explains why the grooves enhanced the compressor stability. The radial transport effect was enhanced, and a larger stall margin improvement was obtained when grooves inclined upstream were applied. The tip flow loss was the dominant loss observed after grooves were applied on the compressor. The grooves with upstream inclination markedly reduced the tip flow loss, indicating that they exhibited the lowest effect on reducing compressor efficiency compared with the other types of grooves.

Keywords: Axial compressor; Casing treatment; Inclination groove; Stability; Tip blockage.

NOMENCLATURE

A	area	SMI	Stall Margin Improvement
B	blockage effect	TE	Trailing Edge
CT	Casing Treatment	r	radial direction
GCT	Groove Casing Treatment	w_r	radial relative velocity
LE	Leading Edge	w_t	circumferential relative velocity
M	mass flow flux	w_z	axial relative velocity
Mo	momentum	γ	loss
MR	Momentum Ratio	θ	circumferential direction
NS	near-stall point	ρ	density
NMF	Normalized Mass Flow rate	π^*	total pressure ratio
PEI	Peak Efficiency Improvement	η^*	rotor efficiency
S	entropy		
SW	Smooth Wall		

1. INTRODUCTION

Challenges in maintaining compressor stability is a major concern during manufacturing of aircraft engines. The compressor mainly exhibits stall and surge, which markedly affect the compressor stability (Benser and Finger 1957; Greitzer 1976).

Several methods have been designed to circumvent the compressor stability problem and enhance the safety of the entire engine system. Several studies have extensively explored casing treatment a potential solution to the compressor stability challenge. Configurations of casing treatment mainly include circumferential grooves and slots. The

circumferential groove has little or no effect on compressor efficiency when used to improve compressor stability compared with use of slots (Moore *et al.* 1971; Osborn *et al.* 1971; Bailey 1972). Rabe and Hah (2002) investigated the potential mechanisms of grooves on enhancing the stability of a transonic compressor. The findings showed a decrease in the flow incidence angle under the interaction effect of tip flows and the flows in grooves, which was a major cause of increase in the stable operation range of the compressor. Shabbir and Adamczyk (2005) conducted a numerical analysis to reveal mechanisms of enhancing compressor stability using circumferential grooves. The results showed that the tip axial momentum has a transport in radial direction after application of the grooves, which is a potential mechanism for improving the compressor stability. Chu *et al.* (2006) conducted numerical simulation and experimental studies to investigate the mechanism of grooves in improving compressor stability. The results indicated that the grooves decreased tip leakage flow ultimately improving the compressor stability. Müller *et al.* (2008) conducted experimental and numerical simulation studies on a transonic compressor to explore the effects of grooves on tip flow structure. The findings showed that the induced vortex was deflected to the suction side, the interaction between vortex and shock was weakened, and blockage area was significantly decreased after application of grooves. The induced vortex was attributed to the tip leakage flows which accumulated near the pressure side of the leading edge of adjacent blades.

The design parameters of grooves have been explored in several studies to further determine the optimal parameters for designing groove casing treatments. Müller *et al.* (2007) investigated the effect of grooves with different depth and axial coverage rates on a single-stage axial compressor using experimental and numerical methods. The results showed that the grooves with a deeper depth or larger axial coverage rate significantly enhanced the stall margin. The findings indicated that potential mechanisms for enhancing flow stability were the effect of the grooves in reducing tip blockage area and weakening the roll-up of tip leakage vortex. Huang *et al.* (2008) explored the effect of different circumferential grooves on NASA Rotor 37 using an in-house CFD code. The effects of axial position, width and depth of grooves on compressor stability were evaluated. The results showed that a large width, an optimal value of the groove depth, and the axial position at 15%-40% chord were effective in improve compressor stability. Sakuma *et al.* (2014) evaluated the effect of circumferential single groove on the stall margin of NASA Rotor 37. The findings revealed that deeper grooves significantly increased the stability margin, and the optimal axial position was near the leading edge of blade. Wu *et al.* (2008, 2009) conducted experimental and numerical simulation analyses to study the effect of axial position, width and depth of grooves on compressor stability. Moreover, an orthogonal analytic method was applied to obtain the groove structure with the highest effect in enhancing compressor stability. In

addition, Chu *et al.* (2008a, 2008b) conducted experimental and numerical investigations to explore the effects of number and width of grooves on compressor stability. Mi *et al.* (2011) studied the effect of three inclined grooves on a subsonic compressor rotor through numerical simulation analyses. The findings indicated that the circumferential grooves with upstream inclination significantly enhanced stall margin and exhibited lower efficiency loss relative to the grooves with downstream inclination. Rolfes *et al.* (2015) reported that the depth, axial extent and inclination of the grooves had insignificant effect on compressor stability compared with the axial position, but the grooves with a slight upstream inclination significantly improved compressor stability. Kim *et al.* (2012) conducted a numerical study to explore the effect of groove shape on compressor performance. The effect of five different groove types, including three different inclined grooves, on NASA Rotor 37 were investigated. The results showed that rectangular grooves with no inclination had the highest effect on enhancing stall margin and showed the lowest efficiency loss compared with the other types. The grooves with downstream inclination showed the weakest ability to enhance compressor stability, and had the highest efficiency loss. Xu (2019) and Xu *et al.* (2019) conducted a numerical simulation study on the effect of three inclined grooves on NASA Rotor 37 on compressor stability and performance. The results showed that the circumferential grooves with downstream inclination exhibited the highest enhancement effect on stall margin of the compressor and had the highest efficiency loss. On the contrary, the circumferential grooves with upstream inclination had the lowest stall margin enhancement effect. Circumferential grooves with no inclination showed the lowest efficiency loss. A review of previous studies on groove casing treatments indicates two shortcomings of studies on enhancing compressor stability. Most previous studies, especially in experimental studies, mainly explored grooves with various depths, widths, and positions rather than evaluating the effect of variation in inclination angle of the grooves. Moreover, the effect and mechanism of inclination grooves on the compressor stability have not been fully elucidated and some studies reported conflicting results.

Therefore, in the current study, the effects of three types of inclination grooves on compressor stability were evaluated through experimental and numerical methods. The main aims of the study were: 1) to explore the effect of inclination grooves CTs on the compressor stability and efficiency using experimental methods; 2) to evaluate the flow mechanism near tip endwall region under application of inclination grooves CTs. The paper comprises the following sections. The first section includes review of review of previous literature on related studies. The research objects, experimental and numerical methods are presented in Section two. The effect of grooves with different inclinations on compressor performance are reported in Section three. The flow mechanism near tip end-wall region under application of different inclination grooves is

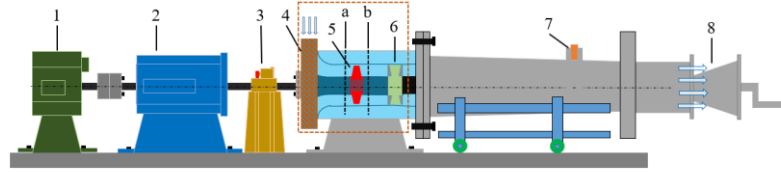


Fig. 1. A representation of the structure of the compressor test rig. a: Rotor inlet probe location; b: Rotor outlet probe location. 1: DC motor; 2: Accelerator; 3: Torque meter; 4: Intake steel cover; 5: Rotor disk; 6: Stator disk; 7: Orifice flowmeter; 8: Throttle valve.

evaluated in Section four. Section five comprises a summary of the main findings.

2. TEST RIG AND RESEARCH METHODS

2.1 Compressor test rig and groove casing treatments

The present investigation was performed on a high-speed subsonic axial compressor test rig. The compressor rotor contained 30 blades characterized by Russia K70 series profile sections. Details on the design parameters of the rotor are presented in Table 1. A representation of the structure of the test compressor rig is shown in Fig. 1. Analyses were performed at approximately 70% design rotating speed. The rotor exhibited the typical tip blockage stall at this speed, which was reported in our previous study (Wu *et al.* 2012).

Table 1 Design parameters of the rotor

Parameter	Value
Design rotating speed (rpm)	15200
Design mass flow rate (kg/s)	5.6
Design total pressure ratio	1.249
Design isentropic efficiency	0.905
Number of blades	30
Casing diameter (mm)	298
Tip clearance/Tip chord	0.011
Hub-tip ratio	0.61

Three types of circumferential groove CTs were designed to evaluate their effects on compressor stability and tip flow structure owing to the cost of the experiment and the size of the test rig. The three circumferential groove CTs had different inclination angles in the axis, and details on their structure are presented in Fig. 2. In the current study, the acronyms GCT_S30, GCT_S00 and GCT_S-30, were used to represent the three groove CTs with 30 degrees downstream inclination, no inclination and 30 degrees upstream inclination. The inclination angle of the grooves facing the blade leading edge is known as the negative inclination angle. The three circumferential groove CTs had four grooves, which covered the whole tip chord, and the axial treatment length of the casing treatment was 21 mm. The axial width and depth of each groove were 4.25 mm and 6 mm, respectively. In the current study, experimental and numerical methods were used to explore the

effects of the three circumferential groove CTs on compressor stability and tip flow structure.

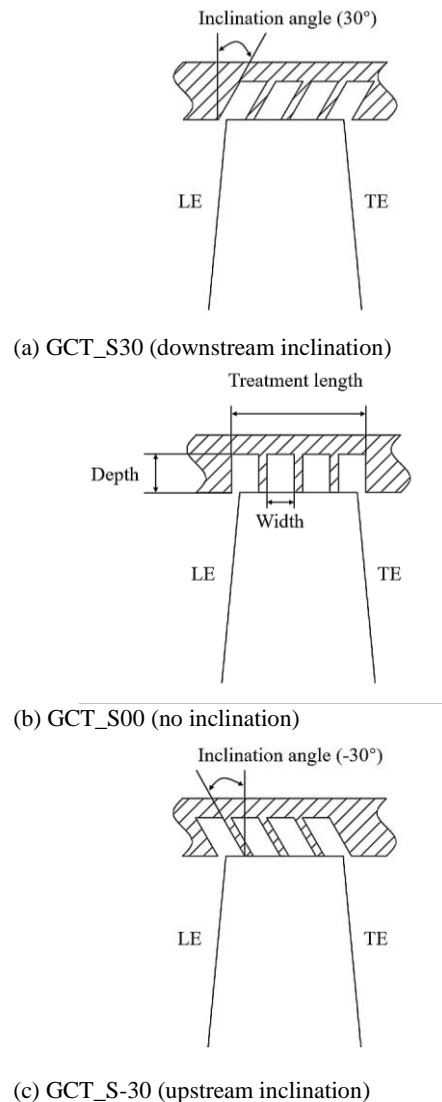


Fig. 2. Structure diagram of groove casing treatments.

2.2 Experimental and Numerical Methods

Experimental investigation was conducted on the subsonic axial compressor test rig. The compressor can operate under different mass flow conditions by controlling the throttle valve. The mass flow rate was determined using an orifice flowmeter at the outlet

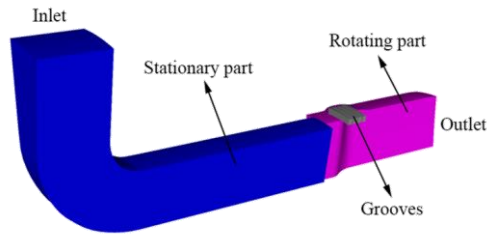
extension section. One three-hole pressure probe was placed at the inlet and another at the outlet measurement plane of the rotor to determine the total pressure ratio performance at different mass flow rates. The torque was measured using a torque meter, and the efficiency was derived from the torque, the rotor speed and mass flow rate.

NUMECA (version 13.2), a computational fluid dynamics (CFD) software, was used for numerical simulations. The numerical calculation was conducted using the unsteady Reynolds averaged Navier-Stokes simulation approach. The Spalart-Allmaras turbulence model was utilized to conduct the simulation. The physical time steps of one rotor blade pitch were set to 20 to achieve a time accurate simulation according to findings from our previous study (Zhang *et al.* 2019). The inlet boundary conditions were set to inlet airflow direction, total pressure and total temperature, and the outlet boundary condition was set to average static pressure. The different compressor operating points were obtained by increasing the average static pressure at the outlet boundary. All solid surfaces were assumed to satisfy no-slip and no-heat transfer conditions. The calculation result was convergent when it satisfied the following criteria: the root mean square of residuals was lower than $1e-5$; the fluctuation of the mass flow rate was less than 0.001kg/s and the relative error between inlet and outlet mass flow rate was less than 0.2% for the last 500 steps; the variation of total pressure and efficiency was less than 0.2% for the last 500 steps.

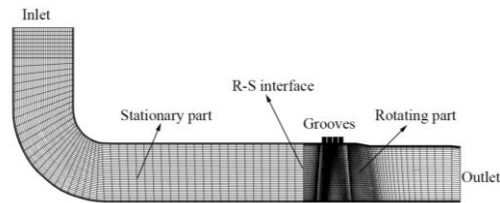
A schematic diagram showing the grids of the single passage numerical simulation model with groove CTs is presented in Fig. 3. The ‘‘H’’ grid topology was adopted in the inlet and outlet extending sections and grooves, whereas ‘‘O’’ grid topology was applied on the rotor blade. The ‘‘butterfly’’ grid topology was adopted in the rotor tip clearance. The number of grids of the whole simulation model was approximately 1.2 million. The grid nodes of rotor passage in the radial, tangential and axial directions were 69, 57 and 233, whereas the grid nodes of each groove in radial, tangential and axial directions were 41, 57 and 21. The y^+ is maintained less than 3. The whole simulation model was divided into two parts. The inlet part was set as the stationary part, whereas the rotor passage, outlet part and grooves were set as the rotating parts. Findings from our previous study on the same compressor rotor (Wu *et al.* 2016) indicated that the turbulence model and the grids adopted in the present study, satisfy the independence condition. The comparisons of the overall performances of CFD and the experimental results are presented in the subsequent section.

3. VARIATION OF COMPRESSOR PERFORMANCE WITH CTS

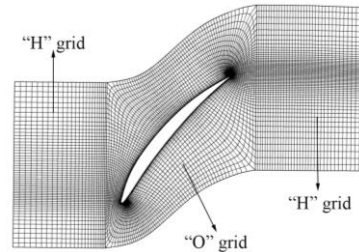
The three designed inclination grooves and smooth wall (SW) were tested using the subsonic axial compressor test rig. The experimental and numerical overall performances of the grooves are shown in Fig. 4. The corrected mass flow rates at different operation points were normalized based on the



(a) A schematic diagram of the numerical simulation model



(b) The grids in the meridian plane



(c) The grids in the rotor passage

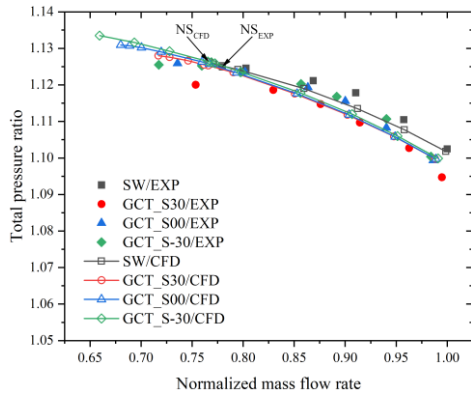
Fig. 3. A schematic diagram and details on the grids of the numerical simulation model.

maximum corrected mass flow rate of SW in the experiment. The normalized mass flow rate (NMF) was expressed as shown in Eq. (1):

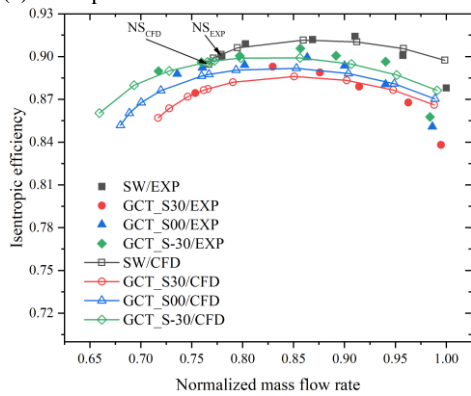
$$NMF = \frac{M}{M_{sw,exp}(max)} \quad (1)$$

where M represents the corrected mass flow rate and $M(max)$ denotes the maximum corrected mass flow rate. The sw and exp subscripts represent smooth wall and experiment. The near-stall points of the SW in the experiment and CFD are indicated in Fig. 4. The findings showed some inevitable differences between the numerical results and experimental results (Fig. 4). However, the total pressure ratio and efficiency obtained from the numerical simulation were consistent with the experimental results in some extent. These parameters showed consistent variation trend and were within the range of error. The numerical mass flow rates at near stall point were lower than of the mass flow rates from experimental results. The effects on stability and efficiency based on the numerical simulation were consistent with the experimental results. The grooves with 30 degrees upstream inclination (GCT_S-30) exhibited the lowest near-stall mass flow rate and the lowest efficiency loss. The grooves with 30 degrees downstream inclination (GCT_S30) showed the highest near-stall mass flow rate and the highest efficiency loss. The present numerical simulation sufficiently revealed some internal flow mechanisms under different inclination groove CTs, despite some

differences between experimental and numerical results.



(a) Total pressure ratio



(b) Isentropic efficiency

Fig. 4. Experimental and numerical results on the overall performance of the rotor.

The stall margin improvement (SMI) and peak efficiency improvement (PEI) were utilized to evaluate the effect of inclination groove casing treatments on compressor stability and efficiency in the present study. The calculations were conducted as shown in equation (2) and equation (3):

$$SMI = \frac{\pi_{ct,ns}^*}{\pi_{sw,ns}^*} \cdot \frac{M_{sw,ns}}{M_{ct,ns}} \times 100\% \quad (2)$$

$$PEI = \frac{\eta_{ct,peak}^* - \eta_{sw,peak}^*}{\eta_{sw,peak}^*} \times 100\% \quad (3)$$

where π^* represents the total pressure ratio, M denotes the corrected mass flow rate, and η^* represents the isentropic efficiency. The ct, sw, ns and peak subscripts represent casing treatment, smooth wall, near-stall point and peak efficiency point, respectively. The NMF at near-stall point, the SMI and the PEI under different casing treatments are presented in Table 2. The findings indicate that the SMI and PEI from the experiments were smaller than those from the numerical simulations. The experimental and numerical results indicated that the grooves with 30 degrees upstream inclination (GCT_S-30) exhibited the highest stall margin improvement and the lowest peak efficiency loss. The grooves with 30 degrees downstream inclination (GCT_S30) had the lowest stall margin improvement and the highest peak efficiency loss. These results

indicate that the grooves with upstream inclination are more effective in further improving the compressor stability, and reducing the efficiency loss caused by grooves.

Table 2 Stall margin improvement and peak efficiency improvement for the different cases

Case	NMF _{ns}	SMI/%	PEI/%
SW/EXP	0.7797	/	/
GCT_S30/EXP	0.7535	3.03	-2.33
GCT_S00/EXP	0.7357	6.08	-1.62
GCT_S-30/EXP	0.7174	8.74	-0.94
SW/CFD	0.7668	/	/
GCT_S30/CFD	0.7171	7.11	-2.80
GCT_S00/CFD	0.6800	13.24	-2.17
GCT_S-30/CFD	0.6593	17.05	-1.37

4. ANALYSIS OF FLOW FIELD IN THE COMPRESSOR

4.1 Stability Enhancing Mechanism of Inclination Grooves

Detailed flow field analyses were conducted to explore the stability enhancing mechanism of the different inclination grooves. All analyses were conducted at a normalized mass flow rate of 0.7668, and at the near-stall point of SW.

4.1.1 Variation in tip loads near tip end-wall region

Static pressure, a common aerodynamic parameter, was applied on the blade suction side and pressure side to represent the variation of tip loads when different inclination grooves were applied on the compressor (Fig. 5). The groove CTs contained four grooves denoted as Groove1, Groove2, Groove3, Groove4 from LE to TE. The static pressure at the pressure side decreased in Groove1, Groove2 and Groove3 after application of groove CTs. The static pressure of the suction side increased in Groove1 and part of Groove2 after application of groove CTs. This implies that the distribution of static pressure difference, which contributes to the tip leakage flow status, changed after application of different inclination grooves. The static pressure difference profiles under different inclination grooves at the same span are shown in Fig. 6. The results showed reduction in static pressure difference in Groove1 and Groove2 sections (about 0-45% axial chord length) after application of groove CTs. This implies that the groove decreased the intensity of tip leakage flow near the leading edge. However, an increase in the static pressure difference was observed behind the position of Groove2. The static pressure difference of GCT_S30 in the Groove2 region was higher than that under other inclination angles. This explains why GCT_S30 exhibited the weakest ability to increase compressor stability.

4.1.2 Variation in tip blockage near the tip end-wall region

Findings from our previous studies indicated that the isolated rotor with SW had the typical tip blockage stall. The tip channel blockage at near stall point,

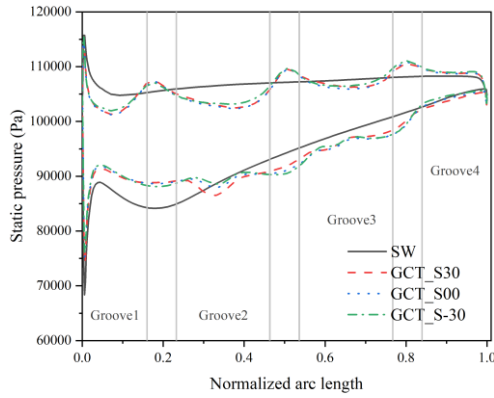


Fig. 5. Static pressure profiles under different groove CTs at 99% span.

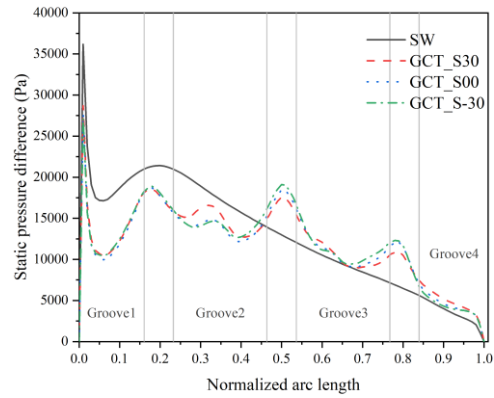


Fig. 6. Static pressure difference profiles under different groove CTs at 99% span.

which is attributed to adverse tip leakage flow, causes stall of the rotor. The static pressure at the pressure side and suction side of the blade tip clearance were different. This pressure difference induces formation of tip leakage flow. Therefore, the change in tip static pressure difference profile promotes a change in the flow structure of the tip leakage flow. The level of tip channel blockage was subsequently changed by the variation of tip flow structure. It is thus imperative to evaluate the level of tip blockage effect. Different studies present different definitions of tip blockage effect. Three distinct quantitative methods were utilized to evaluate the level of tip blockage effect to compare the different definitions of tip blockage effect.

The simplest definition of tip blockage effect is based on the blockage area in which $w_z \leq 0$. A normalized blockage area was thus introduced into this study to evaluate the change in tip blockage under different groove CTs. The normalized blockage area (B_1) is expressed in Eq. (4) and Eq. (5):

$$A_b = \iint_{w_z \leq 0} dA \quad (4)$$

$$B_1 = \frac{A_b}{A} \quad (5)$$

where w_z represents the axial component of relative velocity, A denotes the geometrical section area, and the integration area in which $w_z \leq 0$, and A_b represents the blockage area at different axial positions. The

variation of the tip blockage effect of B_1 is shown in Fig. 7. The results showed that the normalized blockage area of B_1 after application of groove CTs was different compared with that of SW. The GCT_S-30 was the most effective in reducing the tip blockage, resulting in the largest stall margin improvement. The GCT_S00 showed a moderate potential in reducing the tip blockage. Notably, the GCT_S30 increased the tip blockage in most axial positions, and only slightly reduced the tip blockage at 0-15% axial chord length (C_{ax}), 25-40% C_{ax} and 60%-70% C_{ax} positions. This indicates that GCT_S30 had the lowest SMI among the three kinds of groove CTs.

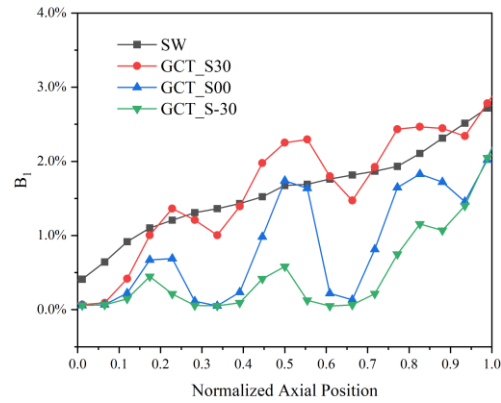


Fig. 7. Variation in tip blockage effect of B_1 under different groove CTs from LE to TE.

These results show that the definition of B_1 can be used to evaluate the level of tip blockage effect. However, B_1 only considers the blockage region in which $w_z \leq 0$, which may result in an imprecise definition of tip blockage. A quantitative method of determination of blockage effect proposed by Choi *et al.* (2011) was used to further evaluate the level of tip blockage effect. The definition of blockage effect (B_2) was expressed shown in Eq. (6):

$$B_2 = \frac{\iint_{\rho w_z \leq \overline{\rho w_z}} \left(1 - \frac{\rho w_z}{\overline{\rho w_z}} \right) dA}{A} \quad (6)$$

where ρ represents the local density, w_z represents the axial component of relative velocity, and A denotes the geometrical section area and the integration area in which $\rho w_z \leq \overline{\rho w_z}$. The variation of B_2 under different groove CTs from LE to TE is presented in Fig. 8. The values of B_2 at different axial positions changed after the application of groove CTs. The B_2 of GCT_S00 and GCT_S-30 was smaller compared with that of SW. The B_2 of GCT_S30 only slightly decreased at 0-15% C_{ax} position compared with that of SW. The B_2 of GCT_S30 increased at 15-100% C_{ax} position compared with that of SW. The B_2 of GCT_S30 may have large deviation for evaluation of tip blockage effect because GCT_S30 extended the compressor by 7.11% SMI as indicated in the CFD and 3.03% SMI as indicated in the experiments. Notably, the value of B_2 could be effectively used to evaluate the ability to extend compressor stability by comparing the B_2 value under the three groove CTs.

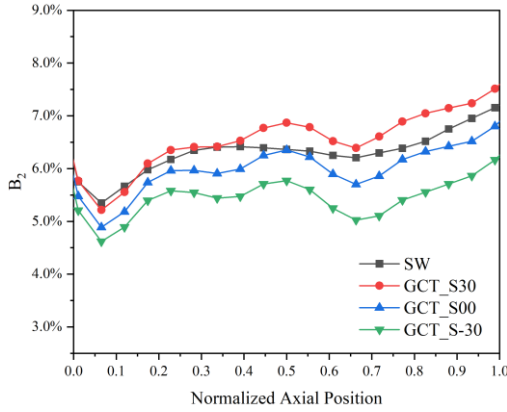


Fig. 8. Variation in tip blockage effect of B_2 under different groove CTs from LE to TE.

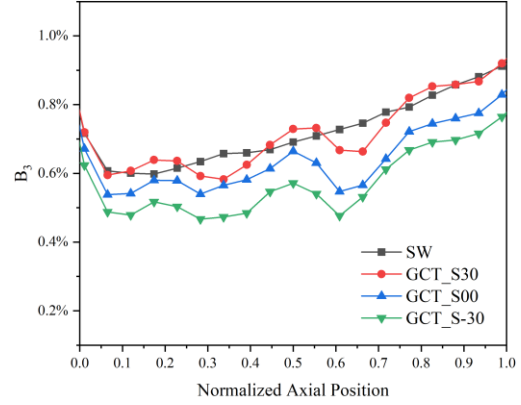


Fig. 9. Variation in tip blockage effect of B_3 under different groove CTs from LE to TE.

A well-defined tip blockage quantitative method was utilized to obtain relatively accurate evaluation of the tip blockage effect. This quantitative method is based on the boundary layer theory (Suder 1998; Liu *et al.* 2013; Berdanier and Key 2018; Wang *et al.* 2022). The tip blockage effect (B_3) was defined as the decrease in effective flow area and was expressed as shown in Eq. (7):

$$B_3 = 1 - \frac{A_{eff}}{A} = 1 - \frac{A - \int \delta^* dr}{A} \quad (7)$$

where A represents the geometrical section area, A_{eff} denotes the effective flow area, r represents the radial direction, and δ^* represents the integral of density-velocity deficit across the blade passage. The δ^* denotes a function of radius and is expressed as shown in Eq. (8):

$$\delta^*(r) = \int_0^{2\pi} \left(1 - \frac{\rho w_z}{\rho w_z} \right) r d\theta \quad (8)$$

where NB represents the number of rotor blade and θ denotes the circumferential direction. The density-velocity deficit region was determined by the sum of radial and circumferential gradients of ρw_z with respect to a suitable cutoff value, and is expressed as shown below:

$$\left| \frac{\partial(\rho w_z)}{\partial r} \right| + \left| \frac{\partial(\rho w_z)}{\partial(r\theta)} \right| \geq cutoff \quad (9)$$

In the present study, a cutoff value of 7000 was used to evaluate the tip blockage effect according to findings from a previous study (Wang *et al.* 2022). The results showed that the blockage near tip end-wall region reduced after application of groove CTs (Fig. 9). The GCT_S30 slightly increased the tip blockage at some axial chord length positions (10%-20% C_{ax} , 45%-55% C_{ax} , 75%-85% C_{ax}), but it significantly decreased tip blockage in most axial positions. This implies that GCT_S30 extended the compressor stability. The GCT_S-30 groove CT was the most effective in reducing the tip blockage, and the GCT_S30 had the lowest ability to reduce the tip blockage. This indicates that the GCT_S-30 had the highest SMI, whereas GCT_S30 had the lowest SMI.

Comparison of the results of the three different definitions of tip blockage effects indicates that the definition of B_3 can be used to accurately evaluate the tip blockage effect. The variation of the tip blockage effect of B_3 was consistent with the extension of the stall margin after application of different groove CTs. This indicates that the reduction of tip blockage by groove CTs was a major mechanism for enhancing compressor stall margin.

4.1.3 Variation in tip flow structure near tip end-wall region

The previous findings indicated that reduction of tip blockage by groove CTs was the major mechanism for enhancing stall margin. Change in tip blockage was ultimately attributed to the variation in tip flow structure caused by the groove CTs, which was mainly manifested as changes in the structure of the tip flow leakage. The tip flow field was analyzed to explore the changes in tip flow structure induced by the different groove CTs. The transient absolute vorticity distribution under different groove CTs at 99% span is presented in Figure 10. The area with the highest absolute vorticity represented the concentration area of the tip leakage vortex. The positions of main flow and tip leakage flow were evident (Fig. 10(a)). The interface between the main flow and tip leakage flow extended across the blade passage at the leading edge impeding the smooth flow of the main flow. The distribution of high absolute vorticity area markedly changed after the application of groove CTs. Analysis of the absolute vorticity distribution showed that the absolute vorticity area with high value in Fig. 10(d) was the smallest among the three types of groove CTs. This shows a weaker potential to impede the flow of the main flow compared with other grooves. The transient tip leakage vortex structures based on the vortex identification criterion (Q criterion) are shown in Fig. 11. The findings indicated that the tip leakage vortex was segmented into several small vortex structures after application of groove CTs on the rotor tip compared with that of SW. The tip leakage vortex exhibited different forms under the effect of the different groove CTs. Notably, the different groove CTs significantly reduced the level of blockage by altering the tip leakage vortex compared with that of SW. The transient tip leakage

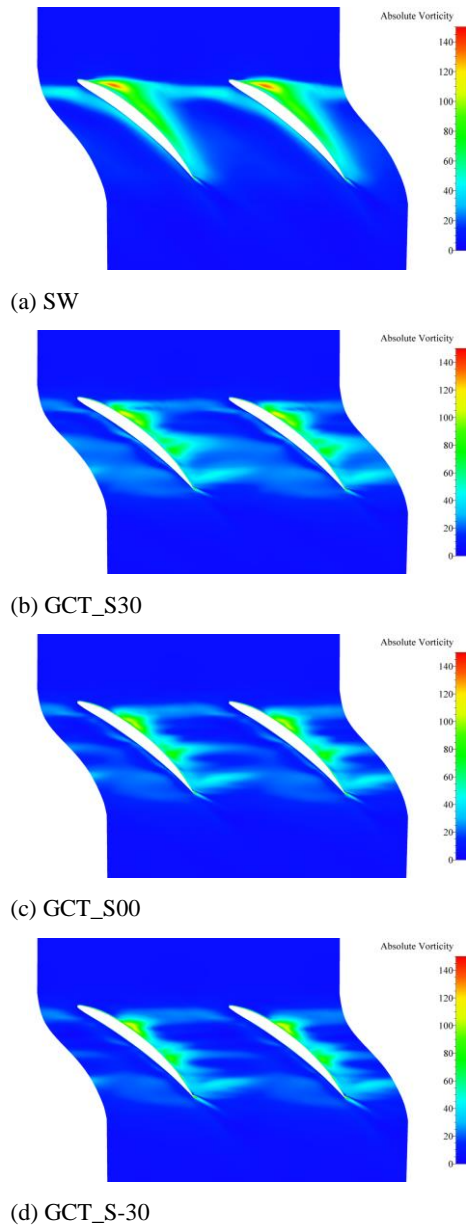


Fig. 10. Transient absolute vorticity distribution under different groove CTs at 99% span.

vortex core structures are shown in Fig. 12. The distribution of the relative Mach number at 99% span under different groove CTs is also presented in Fig. 12. The range of the blue low relative Mach number region was reduced after application of groove CTs. The findings showed that the GCT_S-30 groove type had the highest effect on improving the tip flow field. The trajectory of vortex core showed a deflection towards the suction side after application of the groove CTs. The vortex core was significantly reduced for the GCT_S00 and GCT_S-30 types, which was attributed to the segmented and transport effect of the grooves. An evident vortex core was observed at the tip channel for the GCT_S30 resulting in a significant negative effect on the tip flow field. As a result, the GCT_S30 exhibited the lowest effect in enhancing compressor stability.

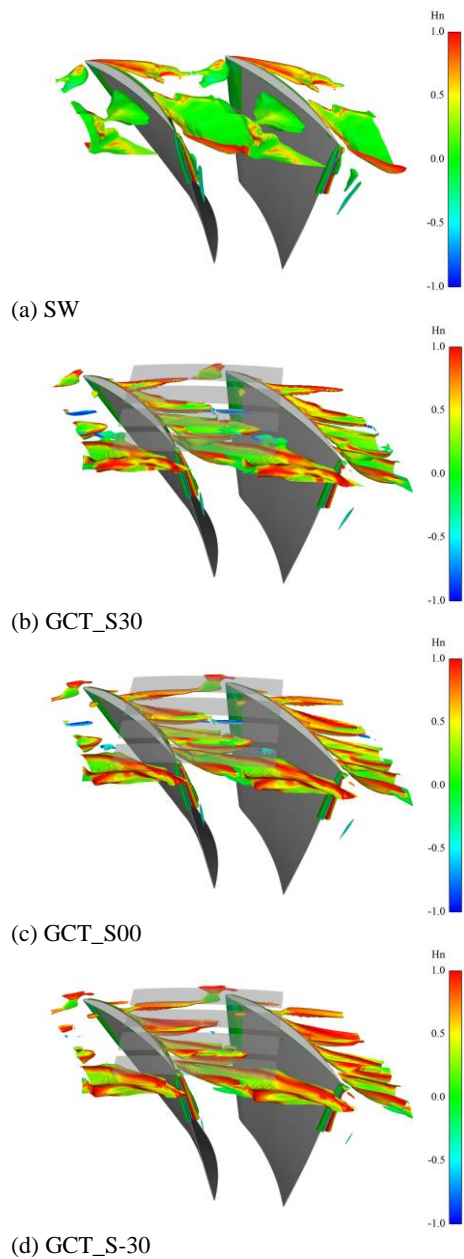


Fig. 11. Transient tip leakage vortex structures under different groove CTs based on Q criterion.

Two aerodynamic parameters were used to describe tip leakage flow to include the alteration in tip leakage flow structure (Fig. 13). The leakage mass flow flux distribution significantly reduced after the application of the groove CTs compared with the leakage mass flow flux of SW (Fig. 13(a)). The reduction level was lower for GCT_S30 compared with that of GCT_S00 and GCT_S-30. However, the level of the reduction for GCT_S00 was similar to that of the GCT_S-30 type. Changes in the tip leakage flow angle are presented in Fig. 13(b). The tip leakage flow angle is defined as the angle between the axial direction and tip leakage flow. The tip leakage flow angle decreased after the application of groove CTs indicating that the tip leakage flow deflected towards the blade suction side. This change improves the flow status of the tip channel and

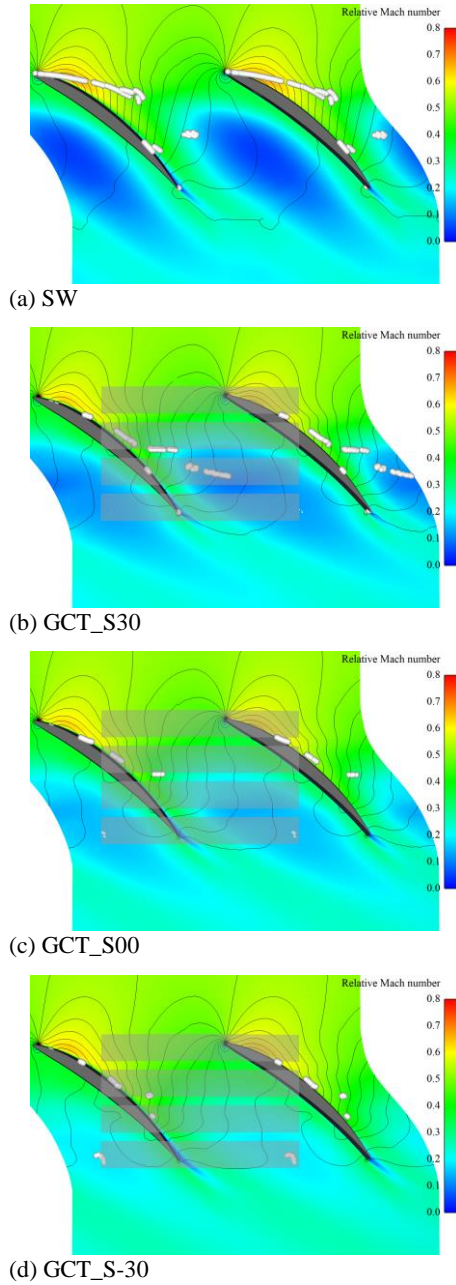
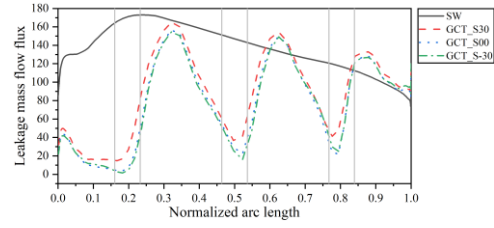


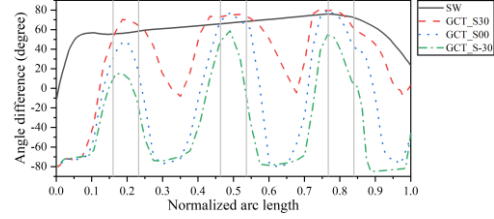
Fig. 12. Transient tip leakage vortex core structures and relative Mach number distribution under different CTs.

alleviates blockage of the tip channel. The GCT_S-30 groove CT exhibited the largest decrease in tip leakage flow angle and had the largest stall margin improvement compared with the other groove CTs.

The findings showed that the tip flow structure in the compressor was modulated by the effect of the groove CTs. As a result, the tip blockage situation was reduced ultimately improving the compressor stall margin. The groove CTs showed different effects on the stability of the compressor rotor due to the different inclination angles of the grooves. In the present study, the grooves with 30 degrees upstream inclination (GCT_S-30) showed the highest effect on enhancing the compressor stability.



(a) Tip leakage mass flow flux distribution



(b) Tip leakage flow angle changes

Fig. 13. Tip leakage flow parameters distribution.

4.1.4 Effect of different inclination grooves on momentum transport

The tip air flow moved in and out of the grooves after application of the groove CTs on the compressor. As a result, a continuous flow interaction occurred between the tip channel and the grooves. The tip flow structure was altered by the flow interaction between the tip channel and the grooves. This flow interaction can be represented by the momentum transport effect. Two parameters, circumferential mass flow flux in groove (M_t) and radial transport momentum of circumferential transport flux (M_{O_r}), were used to quantify the momentum transport effect. The two parameters were expressed as shown below:

$$M_t = \iint \rho w_t dA_1 \quad (10)$$

$$M_{O_r} = \iint \rho w_t w_r dA_2 \quad (11)$$

where A_1 represents the groove section area in the circumferential direction, A_2 denotes the groove bottom area, w_t represents the circumferential component of relative velocity, and w_r represents the radial component of relative velocity. The results showed that the circumferential mass flow fluxes in Groove 1-4 of different groove CTs were not significantly different (Fig. 14). This finding indicates that the circumferential mass flow fluxes of grooves were not significantly affected by the change in inclination angles. This implies that the circumferential mass flow flux in the grooves was not the major mechanism of enhancing the compressor stability. The findings showed that the radial transport effect played an essential role in improving the compressor stability (Fig. 15). The change in inclination angles of the grooves had a significant effect on the effect of the different groove CTs on radial transport. The radial transport effect caused by grooves can effectively alleviate the adverse tip leakage flow. The results showed that the intensity of radial transport effect in Groove 2 and Groove 3 was stronger compared with that of the other grooves. The intensity of radial transport effect in Groove1-4 was highest for the grooves with 30

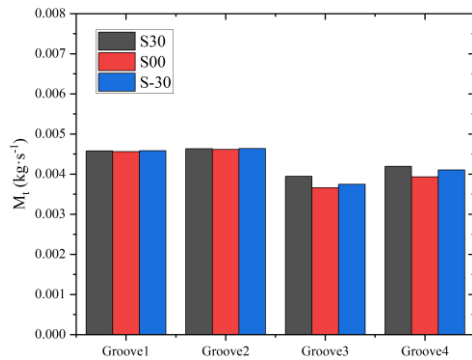


Fig. 14. Circumferential mass flow flux under the different grooves.

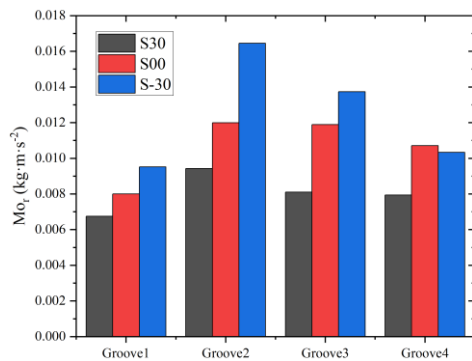


Fig. 15. Radial transport effect under the different grooves.

degrees upstream inclination (GCT_S-30) compared with that of the other two groove CTs. As a result, the GCT_S-30 exhibited the highest ability to enhance the compressor stability. The grooves with 30 degrees downstream inclination (GCT_S30) showed the lowest intensity of radial transport effect, implying that it had the lowest effect in improving stall margin. These results and the results reported in section 4.1.1, section 4.1.2 and section 4.1.3 indicate that the radial transport effect of grooves was a major mechanism in changing the tip flow structure and alleviating tip blockage.

The adverse tip leakage flow can be effectively alleviated under the radial transport effect of the different groove CTs. In addition, the original tip flow dynamic balance state and tip flow structures changed under the different grooves. These changes lead to alteration of tip blockage status. Momentum ratio parameter was introduced in the present study to evaluate the alteration in tip flow dynamic balance state under different groove CTs to determine the momentum balance state. A method reported in a previous study (Du *et al.* 2010) was utilized to evaluate the momentum balance state. Momentum ratio (MR) was expressed as shown in Eq. (12):

$$MR = \frac{Mo_{Tp}}{Mo_{Ic}} \quad (12)$$

where Mo represents the momentum. The I, T, c, p subscripts represent the incoming flow, tip leakage flow, chordwise direction and perpendicular to chordwise direction, respectively. A schematic diagram of the surface for calculation of the

momentum ratio is shown in Fig. 16. Three kinds of operation points of the different groove CTs are presented in Fig. 17. OP1, OP2, OP3 represent the choked point, peak efficiency point, and near stall point of SW, respectively. The results showed that the momentum ratio of the same groove casing treatment gradually increased as the mass flow rate decreased. This implies that the tip leakage flow gradually dominated the tip flow dynamic balance state, and was against the incoming flow. This explains why the tip blockage increased as the mass flow rate decreased. The momentum ratio significantly decreased at the three kinds of operation points after application of the groove CTs. The decrease indicates that the main effect of tip leakage flow reduced under the tip flow dynamic balance state. As a result, the level of tip blockage decreased and the compressor stall margin increased. The GCT_S-30 groove CT showed the most significant decrease in momentum ratio compared with the other grooves. The GCT_S30 groove CT exhibited the least decrease in momentum ratio compared with the other two groove CTs. The change of compressor stall margin was similar to the change in momentum ratio. These findings indicate that the grooves with upstream inclination were more effective in increasing the compressor stability.

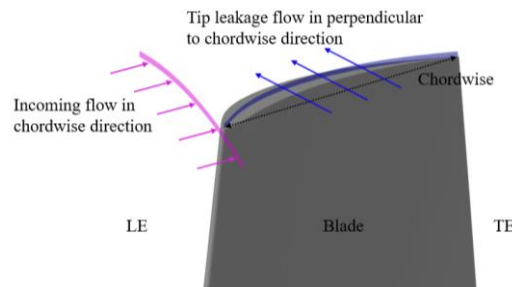


Fig. 16. A schematic diagram of the surface for calculation of momentum ratio.

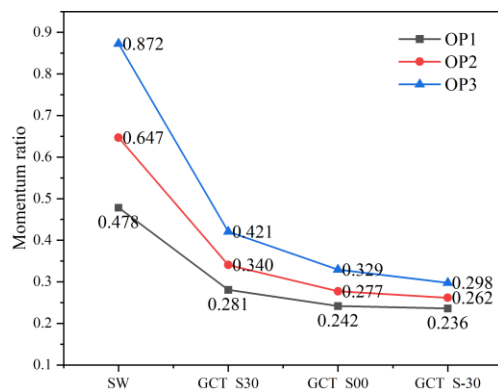


Fig. 17. Variation in momentum ratio under different groove CTs at three operation points.

4.2 Effects of Different Skew Grooves on Compressor Efficiency

The interaction between the flows inside grooves and main flows caused significant flow losses after the application of groove CTs. The distribution of Entropy difference at the meridian plane was used to

evaluate the flow losses after application of the groove CTs (Fig. 18). The entropy difference (ΔS) was expressed as shown in Eq. (13):

$$\Delta S = S_{CT} - S_{SW} \quad (13)$$

where S represents the entropy. The results showed that additional entropy was introduced in the region of grooves. Notably, the entropy difference near tip was different under the different groove CTs. The meridian plane for the GCT_S00 occurred in the positive and negative entropy difference region. The region of negative entropy difference was significantly reduced under the GCT_S30 groove CT, and the positive entropy difference covered most of the parts of the meridian plane (Fig. 18(a)). This implies that the flow loss caused by the GCT_S30 groove CT was larger than the flow loss caused by the GCT_S00 groove CT. However, the region of negative entropy difference was significantly increased under the GCT_S-30 groove CT, and the region of positive entropy difference was reduced (Fig. 18(c)). This implies that the flow loss caused by the GCT_S-30 groove CT was smaller than the flow loss caused by the GCT_S00 groove CT. In summary, the findings indicate that grooves with upstream inclination significantly reduced the flow loss caused by the groove CTs and the grooves with downstream inclination exhibited higher levels of flow loss compared with the other grooves.

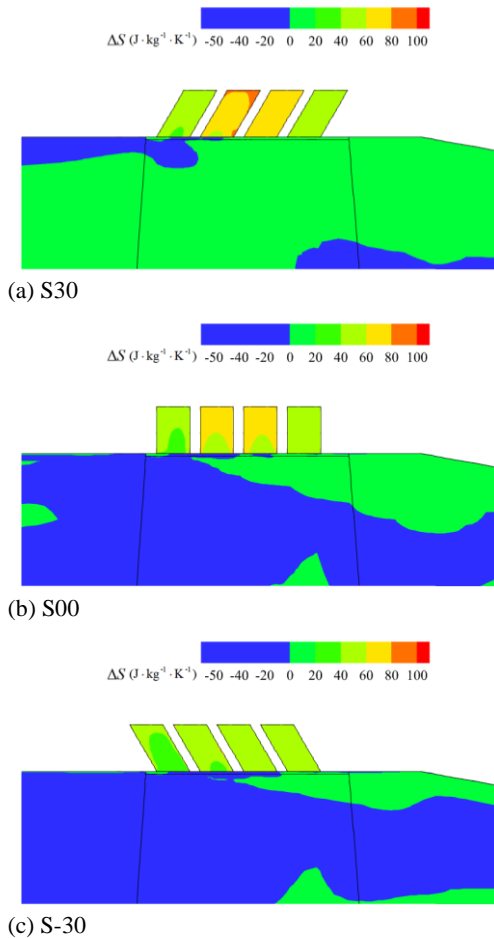


Fig. 18. Entropy difference distribution with different groove CTs.

The integral of entropy at five different regions was calculated to further explore the variation in flow loss at different regions. The compressor passage was divided into five regions to determine the critical region of flow losses caused by the grooves. These five different regions are grouped as shown below:

$$\begin{aligned} \gamma_{in} &: span \geq 2\% span, Z_{in} \leq Z \leq Z_{LE}; \\ \gamma_{out} &: span \geq 2\% span, Z_{TE} \leq Z \leq Z_{out}; \\ \gamma_{hub} &: span \leq 2\% span, Z_{in} \leq Z \leq Z_{out}; \\ \gamma_{tip} &: span \geq 85\% span, Z_{LE} \leq Z \leq Z_{TE}; \\ \gamma_{pas} &: 2\% span \leq span \leq 85\% span, Z_{LE} \leq Z \leq Z_{TE}. \end{aligned} \quad (14)$$

where γ_{in} represents the loss at the inlet region, γ_{out} represents the loss at the outlet region, γ_{hub} represents the loss in hub region, γ_{tip} represents the loss at the tip region, γ_{pas} represents the loss at the passage, Z_{in} denotes the Z -coordinate at the inlet measuring position, Z_{out} denotes the Z -coordinate at the outlet measuring position, Z_{LE} denotes the Z -coordinate at the tip leading edge, and Z_{TE} denotes the Z -coordinate at the tip trailing edge. The results showed that the loss in inlet, outlet and tip significantly changed after application of the groove CTs (Fig. 19). However, the losses in the hub and passage areas did not change after application of the grooves. This implies that application of grooves can cause significant flow loss at the inlet, outlet and tip regions, but has insignificant effect on the passage and hub areas because the groove is distant from these regions. The findings indicate that losses in the outlet and tip regions were the main sources of flow loss in the compressor. The results showed that the tip loss was the main source of flow loss when grooves were applied in the compressor due to the flow interaction that occurred near the tip channel. The GCT_S-30 groove CT exhibited the lowest flow loss in the outlet and tip regions compared with the other groove CTs. This implies that the GCT_S-30 groove CT exhibited the lowest efficiency loss. The GCT_S30 groove CT had the highest loss in the outlet and tip regions, implying that it had the highest efficiency loss on the compressor.

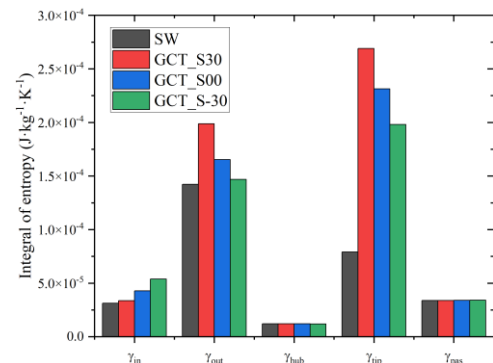


Fig. 19. Variation in the integral of entropy at different regions under different groove CTs.

5. CONCLUSION

In this study, the effect of inclination groove CTs on the compressor stability were investigated through

experimental and numerical simulation methods. The effects of the three different inclination grooves on the compressor stability and the flow structure near the tip end-wall region were explored. The potential mechanism of different inclination grooves was evaluated through analysis of the flow field near the tip end-wall region. The main conclusions of the study are presented below:

1. The investigated compressor rotor exhibited a typical tip blockage stall. The stable operating range of the compressor was extended by application of groove CTs. The experimental results showed that the grooves with no inclination, 30 degrees upstream inclination and 30 degrees downstream inclination exhibited 6.08%, 3.03% and 8.74% SMI. The tip flow structure and tip flow dynamic balance state were altered and redistributed under the radial transport effect of the grooves. Consequently, these changes reduced the tip blockage effect ultimately improving the compressor stability. The reduction tip blockage effect caused by different inclination groove CTs enhanced the compressor stability.

2. The adverse tip leakage flow was effectively alleviated under the radial transport effect of grooves, and the tip flow structure was altered and redistributed. The GCT_S-30 groove CT significantly enhanced the radial transport effect significantly alleviating the adverse tip leakage and the effect of tip leakage flow was markedly reduced in the tip flow dynamic balance state. This indicates that the GCT_S-30 was the most effective in enhancing the compressor stability. However, when the grooves with downstream inclination were applied, the radial transport effect reduced, the ability of alleviation of tip leakage flow by grooves decreased, and the effect of tip leakage flow was stronger. Therefore, the groove casing treatments can be considered with some upstream inclination to obtain larger stall margin improvement.

3. The interaction between the flows inside grooves and main flows caused significant flow losses after application of the groove CTs. The grooves with no inclination, 30 degrees upstream inclination and 30 degrees downstream inclination exhibited -1.62%, -2.33% and -0.94% PEI under experimental conditions. Increase in tip loss was the dominant loss after grooves were applied in the compressor. Different inclination grooves exhibited different effects on the compressor efficiency. The flow losses decreased when grooves with upstream inclination were applied. However, the flow loss increased after application of grooves with downstream inclination. The findings indicate that grooves with upstream inclination should be utilized when designing grooves to minimize flow loss.

ACKNOWLEDGEMENTS

The authors thank for the sponsors by National Natural Science Foundation of China with project No.52076179, and National Major Science and Technology Projects of China No.2017-II-0005-0018.

REFERENCES

- Bailey, E. E. (1972). Effect of grooved casing treatment on the flow range capability of a single-stage axial-flow compressor. *No. NASA TM X-2459*.
- Benser, W. A. and H. B. Finger (1957). Compressor stall problems in gas-turbine-type aircraft engines. *SAE Transactions*, 187-200.
- Berdanier, R. A. and N. L. Key (2018). Demonstrating Multistage Compressor Blockage Calculations Using Pressure Measurements for Large Tip Clearances. *Journal of Propulsion and Power* 34(2), 281-290.
- Choi, M., M. Vahdati and M. Imregun (2011). Effects of fan speed on rotating stall inception and recovery. *Journal of turbomachinery* 133(4), 041013.
- Chu, W. L., X. G. Lu and Y. H. Wu (2006). Numerical and experimental investigations of the flow in a compressor with circumferential grooves. *Journal of Aerospace Power* 21(1), 100-105.
- Chu, W. L., H. G. Zhang, Y. H. Wu and K. J. Ding (2008a). Impact of Grooved Width of Grooved Casing on Stall Margin Improvement. *Acta Aeronautica Et Astronautica Sinica* 29(4), 866-872.
- Chu, W. L., H. G. Zhang, Y. H. Wu and C. N. Dang (2008b). Effects of grooved number of grooved casing treatment on stall margin. *Journal of Propulsion Technology* 29(5), 598-603..
- Du, J., F. Lin, H. Zhang and J. Chen (2010). Numerical investigation on the self-induced unsteadiness in tip leakage flow for a transonic fan rotor. *Journal of turbomachinery* 132(2), 021017.
- Greitzer, E. M. (1976). Surge and rotating stall in axial flow compressors-part I: theoretical compression system model. *Journal of Engineering for Power* 98(2), 190.
- Huang, X., H. Chen and S. Fu (2008). CFD investigation on the circumferential grooves casing treatment of transonic compressor. *In Turbo Expo: Power for Land, Sea, and Air* 43161, 581-589.
- Kim, J. H., K. J. Choi and K. Y. Kim (2012). Performance evaluation of a transonic axial compressor with circumferential casing grooves. *Proceedings of the Institution of Mechanical Engineers, Part A: Journal of Power and Energy* 226(2), 218-230.
- Liu, B. J., Z. B. Zhang and X. J. Yu (2013). Experimental Investigation on Characteristics of Tip Leakage Blockage in an Axial. *Acta Aeronautica et Astronautica Sinica* 12, 2682-2691.
- Mi, P., W. L. Chu, W. Wang and L. Y. Hou (2011).

- Research on the effects of axial inclined circumferential grooves casing treatment on stability extension of compressors, *Chinese Journal of Turbomachinery* 6, 3-7.
- Moore, R. D., G. Kovich and R. J. Blade (1971). Effect of casing treatment on overall and blade element performance of a compressor rotor. *No. NASA-TN-D-6538*.
- Müller, M. W., C. Biela, H. P. Schiffer and C. Hah (2008, January). Interaction of rotor and casing treatment flow in an axial single-stage transonic compressor with circumferential grooves. *In Turbo Expo: Power for Land, Sea, and Air* 43161, 67-78.
- Müller, M. W., H. P. Schiffer and C. Hah (2007, January). Effect of circumferential grooves on the aerodynamic performance of an axial single-stage transonic compressor. *In Turbo Expo: Power for Land, Sea, and Air* 47950, 115-124.
- Osborn, W. M., G. W. Lewis Jr and L. J. Heidelberg (1971). Effect of several porous casing treatments on stall limit and on overall performance of an axial flow compressor rotor. *No. NASA TN D-6537*.
- Rabe, D. C. and C. Hah (2002). Application of casing circumferential grooves for improved stall margin in a transonic axial compressor. *In Turbo Expo: Power for Land, Sea, and Air* 3610, 1141-1153.
- Rolfes, M., M. Lange and K. Vogeler (2015). Experimental investigation of circumferential groove casing treatments for large tip clearances in a low speed axial research compressor. *In Turbo Expo: Power for Land, Sea, and Air* 56635, V02AT37A021.
- Sakuma, Y., T. Watanabe, T. Himeno, D. Kato, T. Murooka and Y. Shuto (2014). Numerical analysis of flow in a transonic compressor with a single circumferential casing groove: influence of groove location and depth on flow instability. *Journal of Turbomachinery* 136(3), 031017.
- Shabbir, A. and J. J. Adamczyk (2005). Flow mechanism for stall margin improvement due to circumferential casing grooves on axial compressors. *Journal of Turbomachinery* 127(4), 708-717.
- Suder, K. L. (1998). Blockage development in a transonic, axial compressor rotor. *No. NASA TM-113115*.
- Wang, X., E. Benini, J. Sun, P. Song and Y. He (2022). Critical endwall blockage attenuation-based automatic optimization of casing treatment design for transonic axial flow compressor. *Aerospace Science and Technology* 107592.
- Wu, Y. H., H. G. Zhang, W. L. Chu and C. N. Dang (2008). Influences of axial positions of grooved casing treatment on stall margin improvement. *Journal of Aerospace Power* 23(7), 1212-1217.
- Wu, Y. H., H. G. Zhang, W. L. Chu and W. J. Deng (2009). Orthogonal experimental investigation of geometry structure of grooved casing treatment. *Journal of Aerospace Power* 24(4), 825-829.
- Wu, Y., Z. Chen, G. An, J. Liu and G. Yang (2016, June). Origins and structure of rotating instability: Part I-experimental and numerical observations in a subsonic axial compressor rotor. *In Turbo Expo: Power for Land, Sea, and Air* 49729, V02DT44A003.
- Wu, Y., Q. Li, J. Tian and W. Chu (2012). Investigation of pre-stall behavior in an axial compressor rotor-Part I: Unsteadiness of tip clearance flow. *Journal of Turbomachinery* 134(5), 051027.
- Xu, A. (2019). *Influence of Casing Treatment on Aerodynamic Characteristics of Transonic Compressor Rotor*. Master's thesis. Civil Aviation University of China, Tianjin, China.
- Xu, A., L. Shi, G. H. Qing, Q. Shi and K. Yao (2019). Influence of inclined circumferential groove casing treatment on flow characteristic of transonic compressor. *Turbine Technology* 61(02), 101-104+157.
- Zhang, H., W. Liu, E. Wang, Y. Wu and W. Yao (2019). Mechanism investigation of enhancing the stability of an axial flow rotor by blade angle slots. *Proceedings of the Institution of Mechanical Engineers, Part G: Journal of Aerospace Engineering* 233(13), 4750-4764.